ACS OMEGA

http://pubs.acs.org/journal/acsodf

Article

Numerical Simulations of Decomposition of Hydrate Particles in Flowing Water Considering the Coupling of Intrinsic Kinetics with Mass and Heat Transfer Rates

Geng Zhang, Jun Li,* Gonghui Liu, Hongwei Yang, and Honglin Huang

Cite This: *ACS Omega* 2021, 6, 23355−23367

Read Online

ACCESS | Metrics & More | Article Recommendations

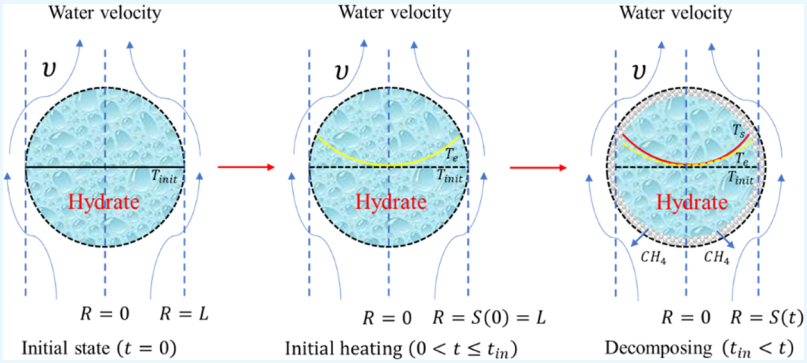

ABSTRACT: During the hydrate exploitation in a shallow marine layer by the mechanical crushing, the hydrate particle decomposition in a wellbore is one of the most concerning problems. In this research, a hydrate dynamic decomposition model coupling intrinsic kinetics with mass and heat transfer rates was established. The model can simulate the hydrate particle decomposition process in flowing water. By comparison, the model calculated results are in good agreement with the measured values. The numerical simulation results show that hydrate decomposition is a non-isothermal process. In the early stage, the hydrate decomposition rate mainly depends on the heat transfer rate. However, it is mainly affected by the hydrate intrinsic kinetics in the late stage. In contrast, the mass transfer rate has little effect on it during the whole decomposition process. By analyzing the influence of sensitivity parameters, it can be found that the activation energy has an important impact on the hydrate decomposition rate, and the hydrate decomposition rate constant decreases significantly at $E/R > 9000$ K. Increasing the water flowing rate is beneficial to the dissolution of hydrates. System temperature and pressure are two significant factors that directly affect the hydrate decomposition rate, and increasing the temperature or reducing the pressure can effectively increase the hydrate decomposition rate.

1. INTRODUCTION

Natural gas hydrates have attracted wide attention in recent years, because they are clean and new energy, and abundant in the seabed. Some countries, such as China and Japan, have carried out a series of pilot mining or mining activities, but the technology is still in its infancy.[1,2] At present, hydrate extraction technology can be divided into two categories: in situ decomposed extraction and in situ crushing extraction. The former includes depressurization technology, thermal excitation technology, carbon dioxide replacement technology, and injection inhibitor technology. The latter includes solid-state fluidization technology and mechanical−thermal combination technology.[3,4]

A shallow marine hydrate reservoir is characterized by low cementation strength and high fragileness. If in situ decomposed extraction technology is adopted, the risk of gas leakage and marine environment pollution is relatively high during the mining process. However, the in situ crushing extraction technology is to break the hydrate into small particles by mechanical crushing, then transport them to the wellhead through a pipeline, and finally carry out postprocessing on the platform,[5−9] which can effectively avoid gas leakage and environmental pollution, as shown in Figure 1. Therefore, the in-situ crushing extraction technology is more applicable to hydrate extraction in shallow marine.

During the hydrate particle transportation process, the hydrate particles decompose due to the increase of temperature

Received: June 14, 2021
Accepted: August 16, 2021
Published: August 28, 2021

https://doi.org/10.1021/acsomega.1c03091
ACS Omega 2021, 6, 23355−23367

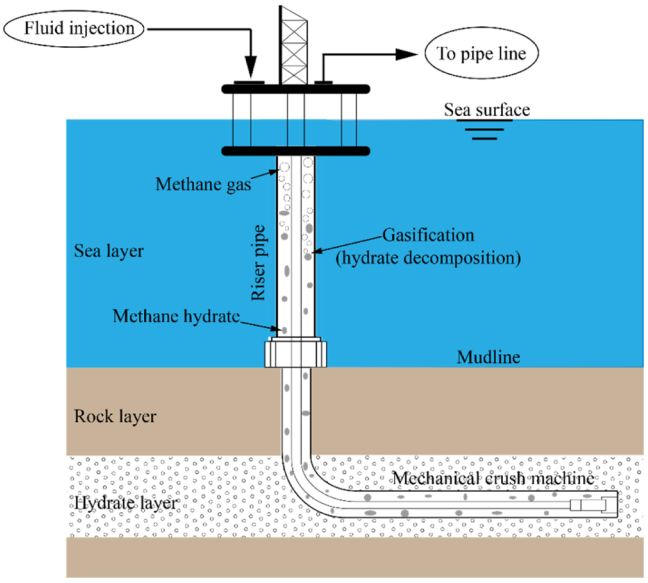

Figure 1. Schematic diagram of in situ crushing exploitation of Marine shallow hydrates.

and decrease of pressure in the wellbore. In the production system, hydrate decomposition will affect the transport efficiency of hydrate particles and wellhead safety. Therefore, it is of great significance to research the decomposition behavior of hydrate particles in the transportation process.

The investigation found that scholars have done much study work on the hydrate decomposition model. Bayles et al.[10] and Holder et al.[11] investigated the hydrate decomposition based on thermodynamics during the process of hydrate thermal excitation mining. Kamath and Holder[12] studied the thermal decomposition process of methane and propane hydrate through experiments. They thought that hydrate decomposition depends on interfacial heat transfer and is analogous to the fluid nucleic boiling. Selim and Sloan[13] studied the pure hydrate block decomposition under constant heat flux. They thought hydrate decomposition is a moving boundary problem, assuming that the gas carries water away from the hydrate surface during the decomposition process. Unfortunately, the models only considered the heat transfer rate, resulting in a large error. Kim et al.[14] built a hydrate decomposition model to describe the hydrate intrinsic decomposition rate based on experiments. They thought hydrate decomposition is a process that involves the particle lattice destruction and the guest molecule desorption. However, the model ignored the effect of heat and mass transfer. Jamaluddin et al.[15] established a new hydrate decomposition model coupling the intrinsic kinetics with the heat transfer rate based on Kim's hydrate decomposition model. Hong et al.[16] established an analytical model to simulate gas production from the hydrate reservoirs under depressure exploitation. They thought that the hydrate decomposition rate depends on heat transfer, intrinsic kinetics, and gas−liquid two-phase flow in porous media. Oyama et al.[17] proposed a hydrate decomposition model based on heat transfer and phase equilibrium.

All the above models mainly described the hydrate in situ decomposition in the reactor and porous media. Besides, some researchers investigated the hydrate decomposition characteristics in the flow state. Sean et al.[18] studied the methane hydrate dissociation process under water flowing conditions by combining experimental observation and CFD numerical simulations. They believed that the hydrate dissociation rate constant does not depend on the flow rate and the system pressure. Hamaguchi et al.[19] deduced the relationship between the Reynolds number and the Nussle number by conducting hydrate decomposition experiments in flowing water. They thought that the decomposing gas will improve the hydrate decomposition rate, when the water temperature is higher than the gas boiling point.

Meanwhile, in oil and gas transportation, some researchers have studied the law of multiphase flow in the process of hydrate slurry transportation. Due to the complexity of hydrate flow in diverse transportation pipelines, scholars mainly use experimental methods to study the characteristics of hydrate flow in gas−liquid two-phase systems. Turner et al.[20] proposed a mechanism model of hydrate formation, slurry flow, and blockage in a three-phase oil−gas−water-mixed transportation system. They divided the process of slurry flow into two categories: emulsification−crystallization−aggregation and adhesion−deposition−clogging. Joshi[21] found the influence of hydrate on the transition of the gas−liquid two-phase flow pattern in the hydrate loop experiment under a high water content. Zerpa et al.[22] established a gas−liquid−solid slug flow model considering hydrates by coupling the hydrate formation model and the slug flow mechanism model. Shi et al.[23] combined the hydrate shell bidirectional growth model with the stratified flow and slug flow mechanism models to construct a quasi-steady-state mechanism model for the stratified flow and slug flow of natural gas-hydrate slurry.

In conclusion, the current hydrate decomposition models mainly depend on Kamath's and Kim's models. However, they ignored the combined effects of the hydrate intrinsic kinetics with heat and mass transfer rates. Meanwhile, these models cannot accurately describe hydrate particle decomposition features in the flow state. In addition, the research on the characteristics of multiphase flow in the process of hydrate transportation mainly focuses on oil and gas transportation and primarily studies the growth, deposition, and blockage of hydrates. There are few studies on the process of hydrate decomposition. Therefore, developing a mathematical model to describe the hydrate decomposition process in flowing water is necessary. In this work, we developed a new mechanism model of hydrate decomposition that coupled the hydrate intrinsic kinetics with the heat and mass transfer rates. The effects of activation energy, water velocity, system temperature, and pressure were analyzed using the built model.

This study will be beneficial for improving the knowledge of the hydrate particle decomposition phenomenon in flowing water and the hydrate decomposition during the hydrate exploitation by mechanical crushing, thus providing a theoretical support for improving the transportation efficiency after hydrate crushing of reservoirs and ensuring the safety of wellheads.

2. MATHEMATICAL MODEL

During the hydrate particles' upward transportation in the wellbore, they will gradually decompose and generate a lot of gas due to the increase of temperature and the decrease of pressure. Then, the decomposed remaining hydrate particles will continue to move upward with the bubbles in the water, as shown in Figure 2. The hydrate decomposition rate is controlled by hydrate intrinsic kinetics and heat and mass transfer rates, and its sensitive parameters include water velocity, hydrate particle size, system temperature, and pressure.

https://doi.org/10.1021/acsomega.1c03091
ACS Omega 2021, 6, 23355−23367

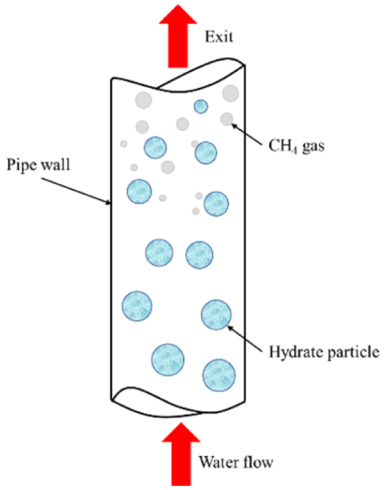

Figure 2. Hydrate particles' upward transport process in a wellbore.

Before establishing the model, the following basic assumptions are made:

(1) The hydrate particles do not rupture and permeate.
(2) Physical parameters of hydrate, such as density, specific heat, and hydrate thermal conductivity, do not change with time and temperature.
(3) The convective heat transfer coefficient does not change with the radius of hydrate particles.
(4) The temperature distribution is symmetric to spherical coordinates in hydrate particles.

2.1. Methane Hydrate Dynamic Decomposition Model. According to Kim's methane hydrate decomposition experimental results,[14] the hydrate decomposition rate is related to the particle surface area, temperature, and pressure. Therefore, the methane hydrate dynamic decomposition model can be expressed as follows

$$\frac{dn}{dt} = A\rho_h \frac{dr}{dt} = -k_{hyd}A[f_{eq}(T_{eq}, p_{eq}) - f(T, p)] \quad (1)$$

The hydrate decomposition rate constant can be determined by the hydrate intrinsic decomposition rate constant and mass transfer rate constant, as shown in the following formula

$$\frac{1}{k_{hyd}} = \frac{1}{k_{hydc}} + \frac{1}{k_{hydf}} \quad (2)$$

According to the Arrhenius equation, the hydrate intrinsic decomposition rate constant calculation formula is as follows

$$k_{hydc} = k_{hydc}{}^0 \, e^{[-E_{act}/(RT)]} \quad (3)$$

2.2. Mass Transfer Process. Figure 3 shows the details of the hydrate particle decomposition process. With the decomposition of hydrate particles, a concentration boundary layer filled with a mixture of methane gas and water will first be generated on the surface of the particles. As the hydrate continues to decompose, the resulting water and gas flow through the particle concentration boundary layer and then diffuse into the surrounding water. The Sherwood number can measure this process. It can be expressed as a function of Reynolds numbers and Schmidt numbers, which can be written as

$$n_{sh} = f(\mathrm{Re}, n_{sc}) \quad (4)$$

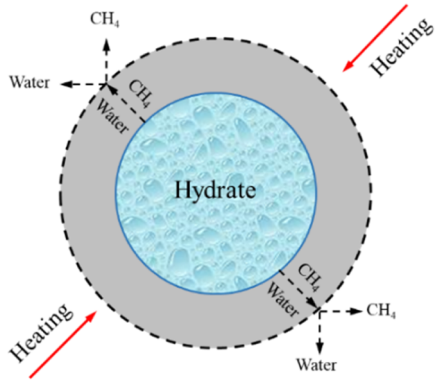

Figure 3. Schematic diagram of the mass transfer process of hydrate decomposition.

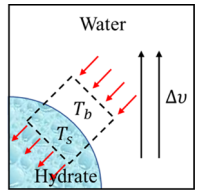

Figure 4. Schematic diagram of heat transfer process between the hydrate particles and water.

Hamaguchi et al.[19] carried out hydrate decomposition experiments under water flow conditions. Meanwhile, they used the lattice gas automata method to simulate hydrate decomposition in flowing water. Finally, they derived the relationship between the Reynolds number and the Schmidt number as follows

$$n_{sh} = 0.347\mathrm{Re}^{0.62} n_{sc}{}^{1/3} \quad (5)$$

According to the related theories of mass transfer, the formulas for the Sherwood number, Reynolds number, and Schmidt number can be obtained as follows

$$\begin{cases} n_{sh} = \dfrac{d_s k_{hydf}{}^0}{D_{AB}} \\ \mathrm{Re} = \dfrac{d_s \nu_l \rho_l}{\mu_l} \\ n_{sc} = \dfrac{\mu_l}{\rho_l D_{AB}} \end{cases} \quad (6)$$

For a very dilute non-electrolyte solution (solvent A+ solvent B), the diffusion coefficient of methane gas in water can be estimated using the Wilke−Chang formula as follows

$$D_{AB} = 7.4 \times 10^{-15} \frac{(\Phi M_B)T}{\mu V_A{}^{0.6}} \quad (7)$$

The mass transfer rate constant of methane gas can be obtained using eqs 5 and 6

$$k_{hydf} = k_{hydf}{}^0 \frac{10^6 p}{Z_g RT} = \frac{0.347\rho_l{}^{0.29}\nu_l{}^{0.62}D_{AB}{}^{0.67}}{\mu_l{}^{0.29}d_s{}^{0.38}} \frac{10^6 p}{Z_g RT} \quad (8)$$

https://doi.org/10.1021/acsomega.1c03091
ACS Omega 2021, 6, 23355−23367

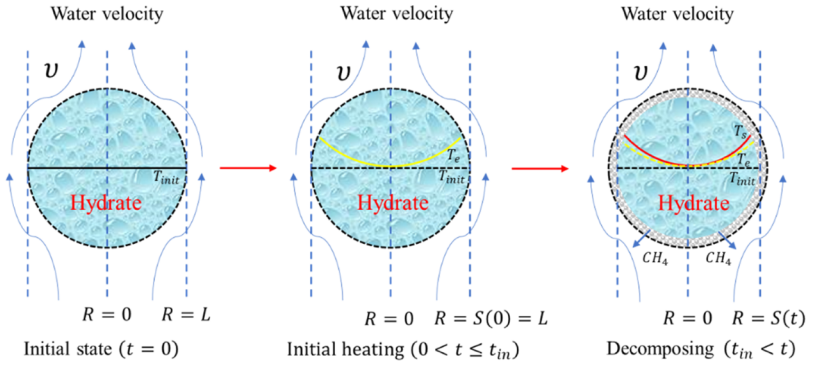

Figure 5. Schematic diagram of the heat transfer process of hydrate particles.

2.3. Heat Transfer Process. It can be seen form Figure 4 that the heat transfer process includes heat conduction inside the particle and heat convection between the hydrate particles and water, when the hydrate particles move in water.

During the hydrate transportation, the temperature distribution of hydrate particles can be divided into the initial state, heating stage, and decomposition stage, as shown in Figure 5. In the initial state, the temperature of hydrate particles is T_{init}. During the heating stage, hydrate particles' surface temperature rapidly reaches the hydrate phase equilibrium temperature T_e. In the decomposition stage, the surface temperature T_s of the hydrate particles depends on the heat conduction of hydrate particles, the heat convection between the hydrate particles and water, and the heat absorption of hydrate decomposition.

The heat conduction inside the hydrate particle depends on the heat conduction equation as follows

$$\frac{\partial(\rho_h c_h T)}{\partial t} = \frac{1}{r^2}\frac{\partial}{\partial r}\left(\lambda_h r^2 \frac{\partial T}{\partial r}\right) + \frac{1}{r^2 \sin^2\theta}\frac{\partial}{\partial \varphi}\left(\lambda_h \frac{\partial T}{\partial \varphi}\right) + \frac{1}{r^2 \sin\theta}\frac{\partial}{\partial \theta}\left(\lambda_h \sin\theta \frac{\partial T}{\partial \theta}\right) + S \tag{9}$$

The heat convection between hydrate particles and water can be measured using the Nusselt numbers, which can generally be expressed as a function of Reynold numbers and Prandtl numbers. Its corresponding relationship is as follows

$$Nu = f(\text{Re}, \text{Pr}) \tag{10}$$

Based on the experimental data, Gao et al.[24] calculated the Nussel number, which is as follows

$$Nu = 0.01215\text{Re}^{0.7922}\text{Pr}^{0.3} \tag{11}$$

The heat absorption of hydrate decomposition can be obtained using the Clausius−Clapeyron equation

$$\frac{\mathrm{d}\ln p_{eq}}{\mathrm{d}(1/T_{eq})} = -\frac{\Delta H_h}{Z_g R} \tag{12}$$

3. NUMERICAL SOLUTIONS

3.1. Governing Equation of Discrete Heat Conduction. In order to clarify the physical concept of the heat conduction partial differential equation and ensure the significance of the dispersion coefficient, the governing equation is discretized by using the finite volume method. Both sides of the governing equation were multiplied by $r^2 \sin^2\theta$, and the heat conduction equation within the control volume, as shown in Figure 6, was integrated as follows

$$\begin{aligned}\int_t^{t+\Delta t}\iiint_V r^2\sin^2\theta\frac{\partial(\rho cT)}{\partial t}\mathrm{d}t\,\mathrm{d}r\,\mathrm{d}\theta\,\mathrm{d}\varphi &= \int_t^{t+\Delta t}\iiint_V \sin^2\theta\frac{\partial}{\partial r}\left(\lambda r^2\frac{\partial T}{\partial r}\right) + \frac{\partial}{\partial\varphi}\left(\lambda\frac{\partial T}{\partial\varphi}\right) \\ &+ \sin\theta\frac{\partial}{\partial\theta}\left(\lambda\sin\theta\frac{\partial T}{\partial\theta}\right)\mathrm{d}t\,\mathrm{d}r\,\mathrm{d}\theta\,\mathrm{d}\varphi \\ &+ \int_t^{t+\Delta t}\iiint_V S\cdot r^2\sin^2\theta\,\mathrm{d}t\,\mathrm{d}r\,\mathrm{d}\theta\,\mathrm{d}\varphi\end{aligned} \tag{13}$$

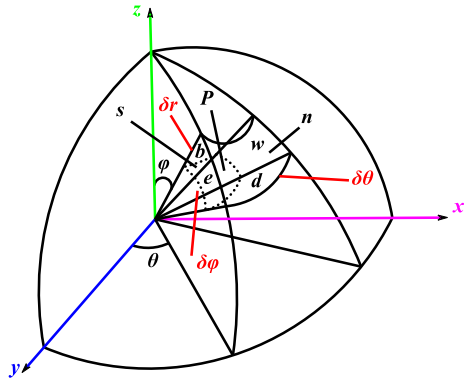

Figure 6. Geometric diagram of the sphere control volume.

Unsteady term integral discretization

$$\begin{aligned}\int_t^{t+\Delta t}\int_s^n\int_w^e\int_b^d r^2\sin^2\theta\frac{\partial(\rho cT)}{\partial t}\,\mathrm{d}t\,\mathrm{d}r\,\mathrm{d}\theta\,\mathrm{d}\varphi &= \frac{(r_n^3 - r_s^3)}{6}(\Delta\theta + \sin\theta_w\cos\theta_w - \sin\theta_e\cos\theta_e)\Delta\varphi(T_p \\ &- T_p^0)\end{aligned} \tag{14}$$

Diffusion term integral discretization in the r direction

$$\begin{aligned}\int_t^{t+\Delta t}\int_s^n\int_w^e\int_b^d \sin^2\theta\frac{\partial}{\partial r}\left(\lambda r^2\frac{\partial T}{\partial r}\right)\mathrm{d}t\,\mathrm{d}r\,\mathrm{d}\theta\,\mathrm{d}\varphi &= \frac{1}{2}(\Delta\theta + \sin\theta_w\cos\theta_w - \sin\theta_e\cos\theta_e)\cdot\Delta\varphi\Delta t \\ &= \left[r_n^2\frac{T_N - T_P}{(\delta r)_n} - r_n^2\frac{T_P - T_S}{(\delta r)_s}\right]\end{aligned} \tag{15}$$

Diffusion term integral discretization in the φ direction

https://doi.org/10.1021/acsomega.1c03091
ACS Omega 2021, 6, 23355−23367

$$\int_t^{t+\Delta t}\int_s^n\int_w^e\int_b^d \frac{\partial}{\partial\varphi}\left(\lambda\frac{\partial T}{\partial\varphi}\right)\mathrm{d}t\ \mathrm{d}r\ \mathrm{d}\theta\ \mathrm{d}\varphi = \left[\frac{T_B - T_P}{(\delta r)_b} - \frac{T_P - T_D}{(\delta r)_d}\right]\Delta\theta\Delta r\Delta t \tag{16}$$

Diffusion term integral discretization in the θ direction

$$\int_t^{t+\Delta t}\int_s^n\int_w^e\int_b^d \sin\theta\ \frac{\partial}{\partial\theta}\left(\lambda\ \sin\theta\frac{\partial T}{\partial\theta}\right)\mathrm{d}t\ \mathrm{d}r\ \mathrm{d}\theta\ \mathrm{d}\varphi = \sin\theta_P = \left[\sin\theta_e\frac{T_E - T_P}{(\delta\theta)_e} - \frac{T_P - T_W}{(\delta\theta)_w}\right]\Delta\varphi\Delta r\Delta t \tag{17}$$

Source term integral discretization:

$$\int_t^{t+\Delta t}\int_s^n\int_w^e\int_b^d r^2\ \sin^2\theta\cdot S\ \mathrm{d}t\ \mathrm{d}r\ \mathrm{d}\theta\ \mathrm{d}\varphi = \frac{(r_n^3 - r_s^3)}{6}(\Delta\theta + \sin\theta_w\cos\theta_w - \sin\theta_e\cos\theta_e)\Delta\varphi\Delta t\ (S_C + S_P T_P) \tag{18}$$

By sorting out the discrete results, the governing equation can be expressed as

$$a_P T_P = a_E T_E + a_W T_W + a_N T_N + a_S T_S + a_B T_B + a_D T_D + b \tag{19}$$

where

$$\begin{cases} a_E = \dfrac{\Delta\varphi\Delta r\ \sin\theta_P\ \sin\theta_e}{\frac{(\delta\theta)_e}{\lambda}}, \\ a_E = \dfrac{\Delta\varphi\Delta r\ \sin\theta_P\ \sin\theta_w}{\frac{(\delta\theta)_w}{\lambda}} \\ a_N = \dfrac{(\Delta\theta + \sin\theta_w\cos\theta_w - \sin\theta_e\cos\theta_e)\Delta\varphi\cdot r_n^{\ 2}}{\frac{2(\delta r)_n}{\lambda}} \\ a_S = \dfrac{(\Delta\theta + \sin\theta_w\cos\theta_w - \sin\theta_e\cos\theta_e)\Delta\varphi\cdot r_s^{\ 2}}{\frac{2(\delta r)_s}{\lambda}} \\ a_B = \dfrac{\Delta\theta\Delta r}{\frac{2(\delta\varphi)_b}{\lambda_d}}, \qquad a_D = \dfrac{\Delta\theta\Delta r}{\frac{2(\delta\varphi)_d}{\lambda_d}}, \\ b = S_C\Delta V + a_P^{\ 0}T_P^{\ 0} \\ a_P = a_E + a_W + a_N + a_S + a_B + a_D + a_P^{\ 0} - S_P\Delta V \\ \Delta V = \dfrac{(r_n^3 - r_s^3)}{6}(\Delta\theta + \sin\theta_w\cos\theta_w - \sin\theta_e\cos\theta_e) \\ a_P^{\ 0} = \dfrac{(\rho c)_P\Delta V}{\Delta t}, \qquad 0 \le \theta \le \pi, \qquad 0 \le \varphi \le 2\pi \end{cases} \tag{20}$$

In order to accurately calculate the surface temperature of hydrate particles, logarithmic grid spacing is used in the radial direction, as shown in Figure 7. The formula is as follows

$$r_i = L(t)\frac{\log(i + i_0)}{\log(m + i_0)} \tag{21}$$

3.2. Initial and Boundary Conditions. The initial conditions are as follows

$$T(r, \theta, \varphi, 0) = T_{\mathrm{init}} \tag{22}$$

The boundary conditions are as follows

$$\begin{cases} \left.\dfrac{\partial T}{\partial r}\right|_{T(0,\theta,\varphi,t)} = 0 \\ h(T_w - T_s) = \lambda\left(\dfrac{\partial T}{\partial r}\right), \qquad r = L(t), \qquad 0 < t < t_{\mathrm{in}} \\ h(T_w - T_s) = \lambda\left(\dfrac{\partial T}{\partial r}\right) - \rho_{\mathrm{H}}M_{\mathrm{H}}\Delta H_{\mathrm{hyd}}\dfrac{\mathrm{d}r}{\mathrm{d}t}, \\ \quad r = L(t), \qquad t \ge t_{\mathrm{in}} \end{cases} \tag{23}$$

3.3. Auxiliary Equation. Based on the definition of pure material fugacity, the calculation formula of methane gas fugacity can be derived by using the Redlich−Kwong (R−K) equation

$$\ln\varphi = \ln\left(\frac{f}{p}\right) = Z - 1 - \ln\left(Z - \frac{pb}{RT}\right) - \frac{a}{bRT^{1.5}}\ln\left(1 + \frac{b}{V}\right) \tag{24}$$

The calculation formula of the coefficient of the R−K equation is as follows

$$\begin{cases} a = \dfrac{0.72748\cdot R^2\cdot T_c^{2.5}}{p_c} \\ b = \dfrac{0.08664\cdot R\cdot T_c}{p_c} \end{cases} \tag{25}$$

According to the comparison form of the R−K equation, the calculation formula of the methane gas compression factor is derived as follows

$$\frac{1}{Z\left(1 - 0.08664\frac{p_r}{ZT_r}\right)} - \frac{0.42747p_r}{Z^2T_r^{2.47}\left(1 + 0.08664\frac{p_r}{ZT_r}\right)} = 1 \tag{26}$$

The phase equilibrium temperature can be obtained by using the hydrate phase equilibrium model established by Dzyuba and Zektser,[25] as shown below

$$T_{\mathrm{eq}} = 9.6339\ln p_{\mathrm{eq}} + 264.9661 \tag{27}$$

3.4. Solution Process. We adopted the finite volume method to discretize the control equation of the model. Meanwhile, we used the logarithmic grid to discretize the control body. We discretized all control units and obtained a set of seven-diagonal linear equations. In this paper, we used the Gauss−Seidel iterative method to solve the equations. The flow chart of the entire solution process shown in Figure 8 and the detailed calculation steps are as follows:

1. Enter the thermophysical parameters such as hydrate density, heat capacity, and thermal conductivity, as well as basic parameters such as hydrate particle radius, water flow velocity, and pipe diameter.
2. Input the initial temperature and pressure, divide the space grid, and discretize the control equation.

https://doi.org/10.1021/acsomega.1c03091
ACS Omega 2021, 6, 23355−23367

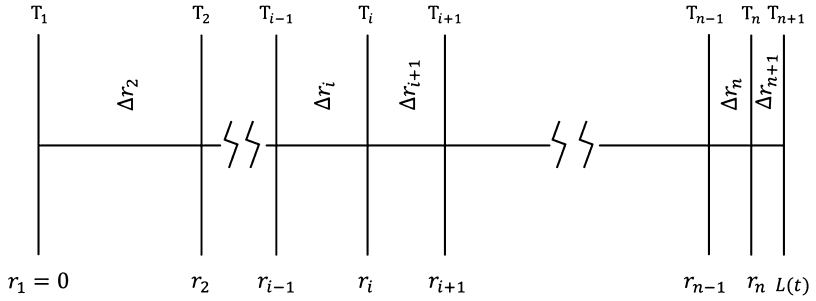

Figure 7. Schematic diagram of the radial logarithmic grid.

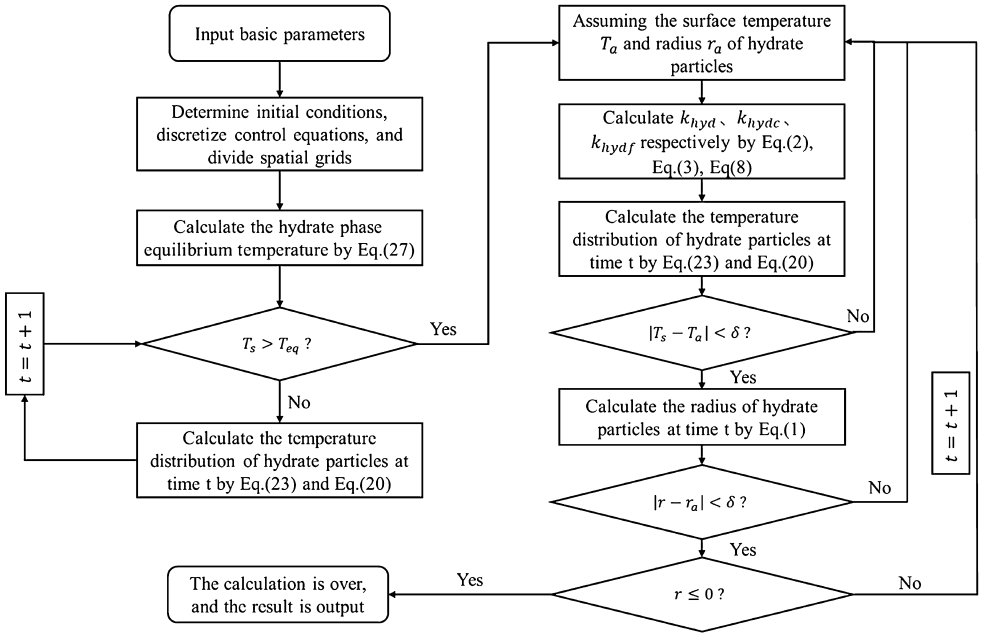

Figure 8. Flow chart of the model.

3. Use Formula 27 in the manuscript to calculate the hydrate phase equilibrium temperature T_{eq}. Determine whether the surface temperature of the hydrate particle reaches the critical temperature of hydrate decomposition.
4. If $T_s < T_{eq}$, it means that the hydrate particles have not yet begun to decompose. We used the boundary conditions in Formula 23 to solve the linear eq 20 and obtained the temperature distribution T of the hydrate particles at time t. Then, return to step 3 and calculate the temperature of hydrate particles at time $t + 1$.
5. If $T_s > T_{eq}$, it means that the hydrate particles have decomposed. Assume the surface temperature T_{assume} and the radius T_{assume} of the hydrate particles.
6. Use Formulas 2, 3, 8 in the manuscript to calculate the intrinsic dynamic rate constant, mass transfer rate constant, and hydrate decomposition rate constant, respectively.
7. Use eqs 20 to calculate the temperature distribution of hydrate particles to determine whether the surface temperature of hydrate particles meets the accuracy requirements, that is, $|T_s - T_{assume}| < \delta$.
8. If the surface temperature of the hydrate particles satisfies $|T_s - T_{assume}| < \delta$, the temperature distribution of the hydrate particles at time t is correct, otherwise, return to the step 5 for correction.
9. According to the calculated temperature distribution of hydrate particles, use Formula 1 to calculate the radius r of the hydrate particles at time t. Determine whether the radius of the hydrate particles meets the accuracy requirements that is $|r - r_{assume}| < \delta$.
10. If the radius of the hydrate particles satisfies $|r - r_{assume}| < \delta$, the calculation of the radius of the hydrate particles at time t is correct, otherwise, return to the step 5 for correction.
11. Determine whether the hydrate particles wholly decomposed. If $r \geq 0$, it means that the hydrate particles have not entirely decomposed, and the calculation is over at time t. We need to update the grid nodes and return to step 5 to calculate the time $t + 1$.
12. If $r < 0$, it means that the hydrate particles are all decomposed, and the calculation ends. Then, output the calculation result.

4. MODEL VALIDATION

In this paper, the developed dynamic decomposition model of hydrate was verified by using the experimentally measured data. We compared the calculation results of the model with the experimental results of Hamaguchi et al.[19] They tested the decomposition rate of hydrate particles when the system temperatures were 295, 297, 308, and 310 K. The water flow

https://doi.org/10.1021/acsomega.1c03091
ACS Omega 2021, 6, 23355−23367

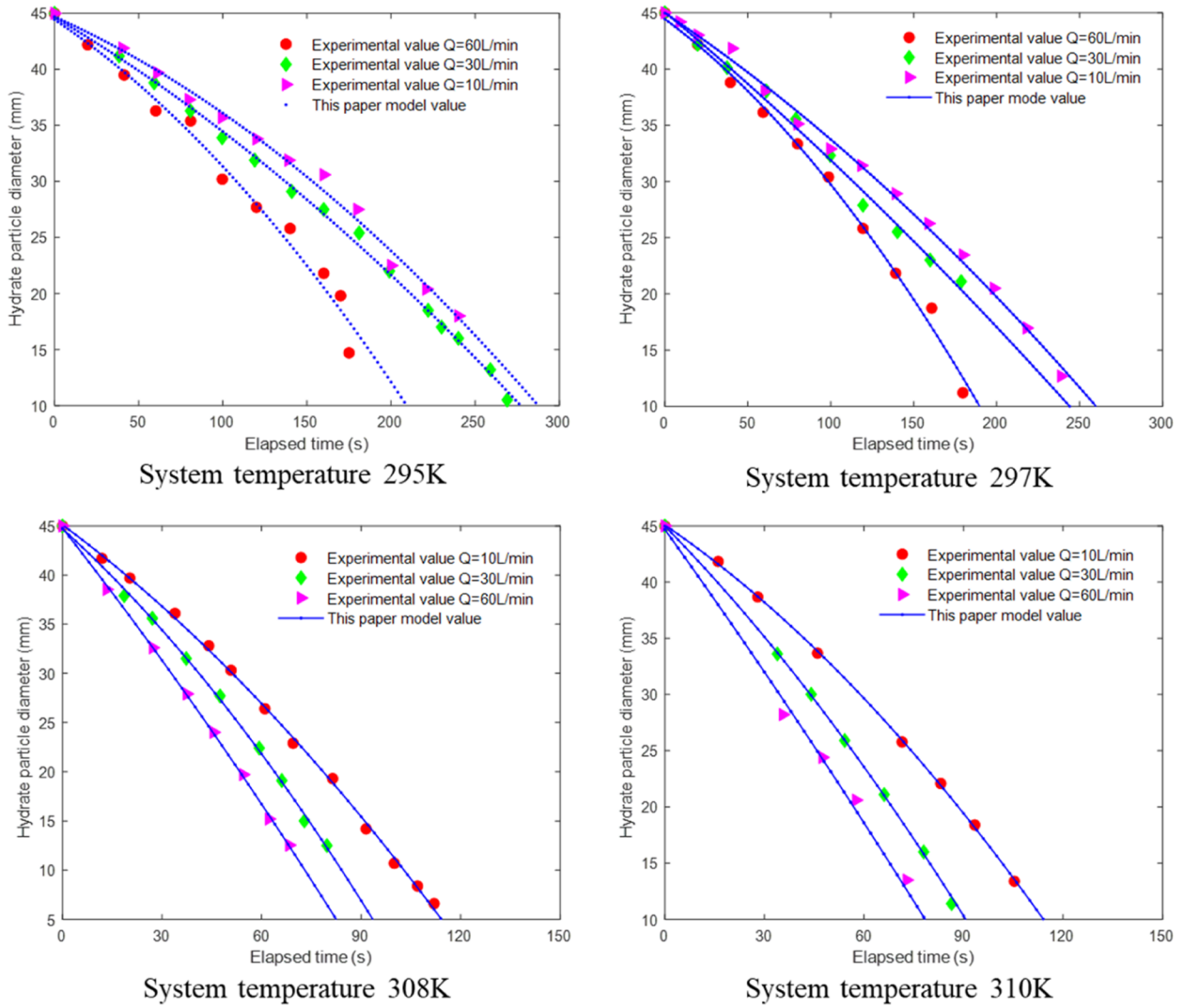

Figure 9. Comparison of the measured and calculated results. Reprinted with permission from [Hamaguchi, R.; Nishimura, Y.; Inoue, G.; Matsukuma, Y.; Minemoto, M. Gas hydrate decomposition rate in flowing water. *J. Energ. Resour-Asme.* **2007**, *129*, 102−106]. Copyright [2007] [*J. Energ. Resour-Asme*].

rates were 10, 30, and 60 L/min. We compared the experimental results with the model calculation results, as shown in the figure below. It is easy to find from Figure 9 that the calculation results of the model in this paper are in good agreement with the experimental results, which further proves the model's accuracy. The experimental relevant parameters are shown in Table 1.

Table 1. Experimental Relevant Parameters

parameter	value
initial temperature of hydrate particles	280 K
initial diameter of hydrate particles	45 mm
experimental system temperature	295 K
experimental system pressure	0.1 MPa
experimental glass square pipe dimensions	80·80·800 mm

In addition, the calculation results of the new model were compared with those of the Kim model[11] and Jamaluddin model,[12] whose results are shown in Figure 10. The figure shows that the calculated results of the new model are closer to the experimental results. The calculated results of the Kim model and Jamaluddin model deviate from the experimental results to a certain extent, among which the computed results of the Kim model have more error. The main reason is that the Kim model only considered the intrinsic kinetics of hydrate, but regarded hydrate decomposition as an isothermal reaction. The Jamaluddin model ignored the mass transfer resistance of the decomposed gas. At the same time, we can find that the calculation result of Jamaluddin model is closer to the experimental measurement value than the Kim model, that is to say, the effect on the decomposition rate of the heat transfer rate is more significant than the mass transfer rate. This further proves the accuracy of the model.

5. RESULTS AND DISCUSSION

A series of numerical simulations were carried out using the established model to research heat and mass transfer processes, and the hydrate particle decomposition in flowing water. The simulation parameters are shown in Table 2.

5.1. Results. Through a series of numerical simulations, the hydrate particle decomposition behavior in flowing water is studied. In the process of simulations, it is assumed that the hydrate particle is suspended in the pipeline in a balanced state without settling.

https://doi.org/10.1021/acsomega.1c03091
ACS Omega 2021, 6, 23355−23367

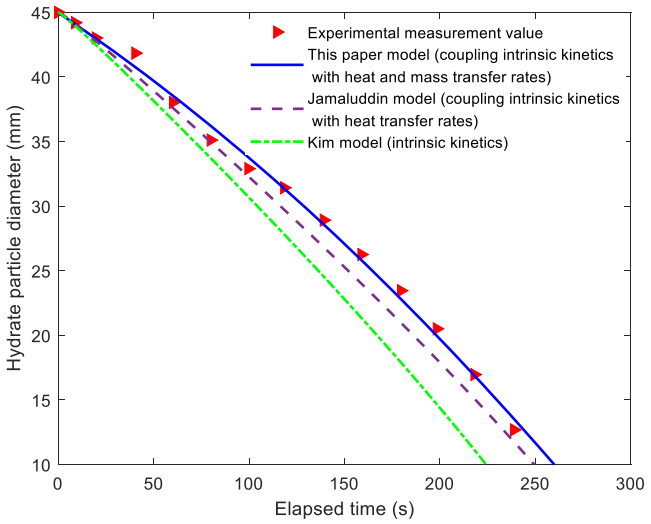

Figure 10. Comparison of the model reported in this paper and the model of Kim and Jamaluddin. Reprinted with permission from [Kim, H. C.; Bishnoi, P. R.; Heidemann, P. A.; Rizvi, S. S. H. Kinetics of methane hydrate decomposition. *Chem. Eng. Sci.* **1987**, *42*, 1645−1653]. Copyright [1987] [*Chem. Eng. Sci*]; Reprinted with permission from [Jamaluddin, A. K. M.; Kalogerakis, N.; Bishnoi, P. R. Modeling of decomposition of a synthetic core of methane gas hydrate by coupling intrinsic kinetics with heat transfer rates. *Can. J. Chem. Eng.* **1989**, *67*, 948−954]. Copyright [1989] [*Can. J. Chem. Eng*].

Table 2. Simulation Parameters

parameters	values
system temperature	310 K
system pressure	7 MPa
initial diameter of the hydrate particles	40 mm
initial temperature of the hydrate particles	273 K
water flowing rate	30 L/min
hydrate particle density	0.0083 mol/cm^3
hydrate particle heat capacity	255 J/(mol·K)
hydrate particle thermal conductivity	0.005 W/(cm·K)
hydrate number	5.75
hydrate intrinsic rate constant	1.56396×10^9 cm/(MPa·s)
activation energy	78300 J/mol
Universal gas constant	8.314 J/(mol·K)
pipe diameter	80 mm

It is easy to see from Figure 11 that in the early stage of decomposition of hydrate particles, the surface temperature and decomposition rate of hydrate particles increase sharply. As the hydrate particles continue to decompose, the surface temperature of the hydrate particles gradually stabilizes. On the contrary, due to the decrease of the diameter of hydrate particles, the dissociation surface area decreases, leading to the gradual decline of the hydrate decomposition rate. Therefore, we can realize that the heat transfer efficiency on the surface of hydrate particles dominates in the early stage of decomposition of hydrate particles. When the surface temperature of the hydrate particles gradually stabilizes, the intrinsic power of the hydrate plays a significant role. In addition, due to the higher temperature of the hydrate particles, the gas diffusion coefficient is larger. The gas generated by the decomposition rarely accumulates on the surface of the hydrate particles, so the mass transfer resistance has little effect on the decomposition rate of the hydrate.

The temperature distributions of hydrate particles at different times are shown in Figure 12 and 13. The temperature of hydrate particles increases gradually along with the radius from the inside to the outside. At the same time, with the increase of time, the hydrate particles continue to shrink, and the overall temperatures increase and gradually approached the water temperature. This further indicates that hydrate decomposition is not an isothermal process, and the heat transfer rate of hydrate particles cannot be ignored.

The change law of rate constant during hydrate decomposition is studied, and the results are shown in Figure 14. With the increase of time, the hydrate decomposition rate constant and intrinsic rate constant increase gradually, while the mass transfer rate constant decreases gradually, which is mainly due to the increase of surface temperature of hydrate particles, which leads to the decrease of mass transfer resistance of methane gas. Besides, we can find that the intrinsic kinetics plays a dominant role in the hydrate decomposition process, and the mass transfer rate has little effect on the hydrate decomposition rate.

5.2. Discussion. During mining shallow marine hydrate by in situ crushing extraction, the characteristics of hydrate particle decomposition during pipeline transportation have an important influence on the exploitation system's safety and the economic rate of return. Therefore, to further understand the decomposition of hydrates in the flowing water, we studied the effects of sensitive parameters such as activation energy, particle diameter, system temperature, and pressure on the particle diameter, surface temperature, and decomposition rate constant during the hydrate decomposition process.

5.2.1. Influence of the Activation Energy. The activation energy has an important influence on the hydrate decomposition rate. Kim et al. (1987) estimated the activation energy of methane hydrate decomposition reaction based on the experimental data and concluded that the value of E/R was about 8700 K. Therefore, A and B were used to compare and analyze the influence of activation energy on hydrate decomposition. Therefore, the E/R values of 8000, 8500, 9000, and 9500 K were used for comparative analysis to explore the influence of activation energy on hydrate decomposition.

It can be seen from Figure 15 that, with the increase of activation energy, the shrinkage rate of hydrate particle diameter slows down significantly, indicating that the hydrate decomposition rate decreases. Simultaneously, with the increase of activation energy, the hydrate decomposition rate constant decreased significantly, especially when $E/R > 9000$ K, as shown in Figure 16. It can be seen from Figure 17 that the higher activation energy, the higher the surface temperature of hydrate particle. Besides, we can find that when the activation energy is low, the decomposition rate of hydrate is mainly controlled by the intrinsic kinetics. In contrast, when the activation energy is high, the hydrate decomposition rate is jointly determined by the intrinsic kinetics and the heat and mass transfer rates.

5.2.2. Influence of the Water Velocity. Through numerical simulations, it is found that the water velocity has a significant influence on the hydrate decomposition rate. As can be seen from Figure 18, with the increase of flowing rates, the heat convection on the surface of hydrate particles increases, the heat transfer rate increases, and the surface temperature of hydrate particles increases accordingly. The increase of the surface temperature of hydrate particles accelerates the decomposition of hydrate particles. It can be clearly seen from Figure 19 and 20 that the hydrate decomposition rate constant and the rate of particle diameter shrinkage increase. Besides, the increase of

https://doi.org/10.1021/acsomega.1c03091
ACS Omega 2021, 6, 23355−23367

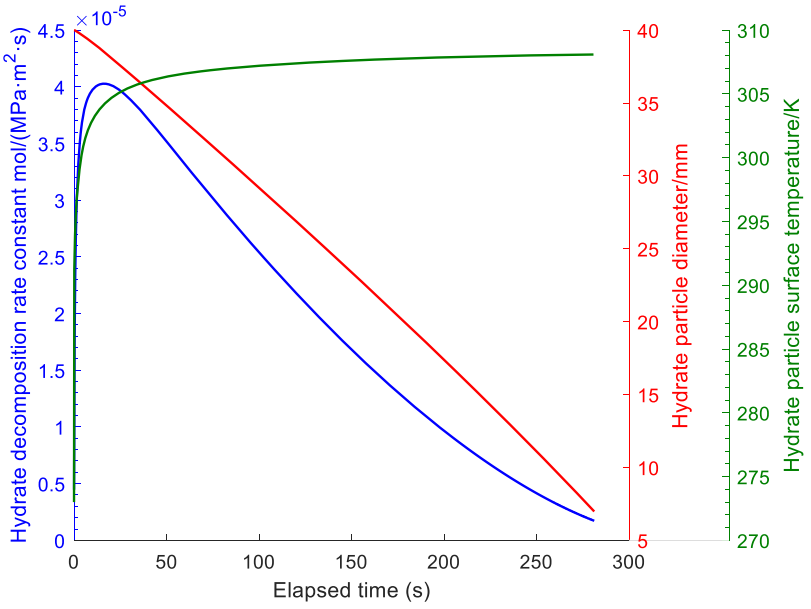

Figure 11. Hydrate particle diameter, surface temperature, and the decomposition rate vary with elapsed time.

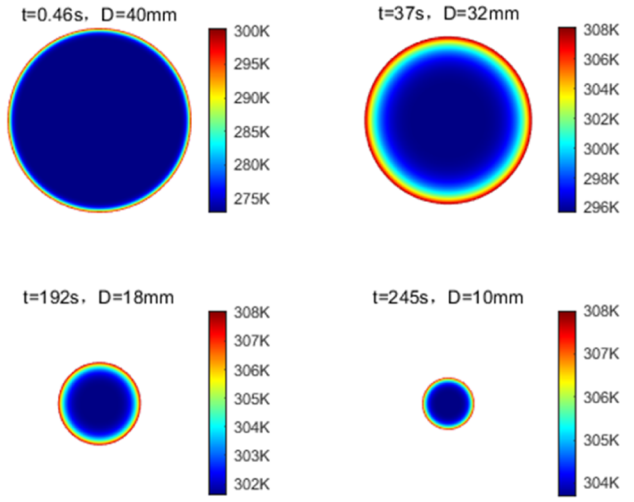

Figure 12. Cloud image of the hydrate particle diameter and temperature at different decomposition times.

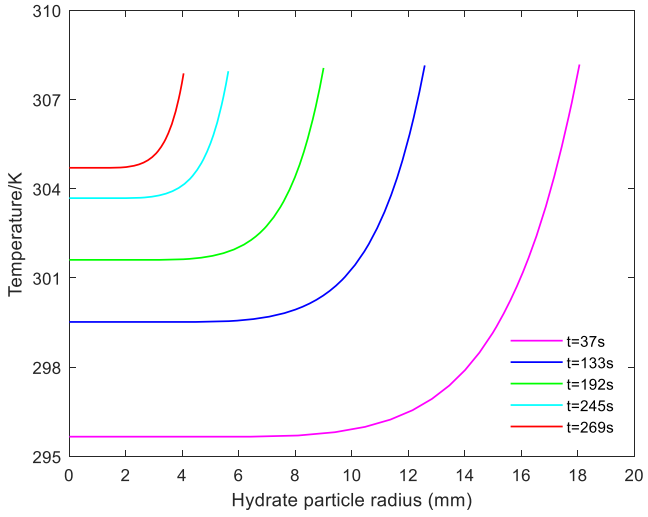

Figure 13. Temperature of hydrate particles varies along with the radius at different decomposition times.

water velocity also promotes the gas mass transfer process so that the mass transfer rate increases, thus enlarging the hydrate decomposition rate.

5.2.3. Influence of the System Temperature. It is well known that system temperature is one of the critical factors affecting the hydrate decomposition rate. The higher the system temperature is, the higher the heat transfer rate will be. Furthermore, hydrate particles' surface temperature will increase correspondingly, which will eventually promote the increase of the hydrate decomposition rate constant and the particle diameter reduction rate, as shown in Figures 21, 22, and 23. Besides, with the increase of system temperature, the mass transfer resistance of methane gas decreases continuously, which leads to the increase of the gas mass transfer rate in the process of hydrate decomposition, and accordingly promotes the decomposition of hydrate.

5.2.4. Influence of the System Pressure. The calculation results show that, as expected, the system pressure significantly affects the hydrate decomposition rate. It can be seen from Figures 24 and 25 that the lower the system pressure, the higher the shrinkage rate of the hydrate particle diameter and the hydrate decomposition rate constant. This further indicates that pressure is the main driving force of hydrate decomposition and depressure-induced hydrate decomposition is one of the main methods to extract hydrate. Besides, it is worth noting that for the hydrate, the surface temperature of particles increases with the decrease of pressure, as shown in Figure 26 which is mainly because hydrate decomposition is an endothermic reaction. The higher the hydrate decomposition rate, the more heat absorbed, and the lower the surface temperature of hydrate particles.

6. CONCLUSIONS

Based on the intrinsic kinetics of hydrates, a dynamic decomposition model of hydrates in flowing water was established considering the coupling effects of heat and mass transfer rates. The decomposition process of hydrate particles in flowing water was investigated by using the established model. Moreover, the influence of sensitive parameters such as

https://doi.org/10.1021/acsomega.1c03091
ACS Omega 2021, 6, 23355−23367

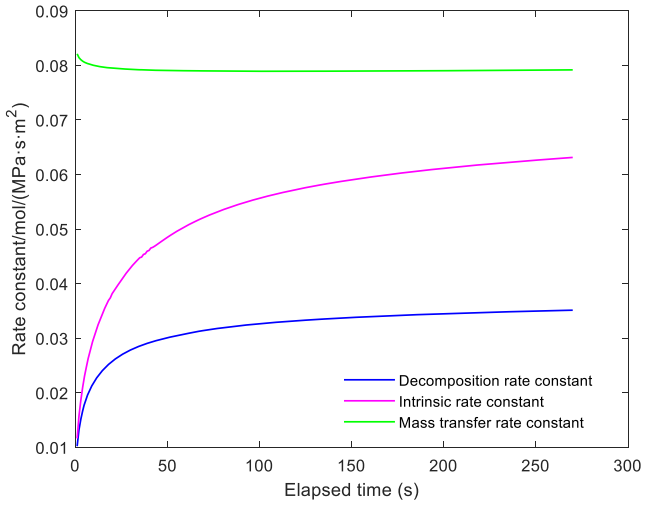

Figure 14. Relation curve of different rate constants with time.

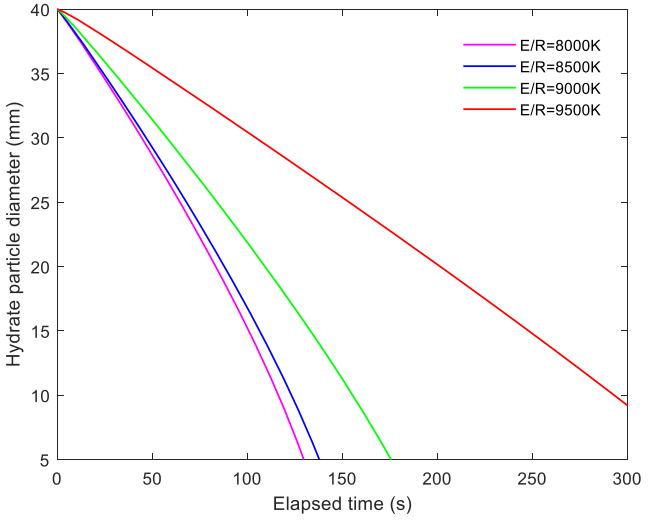

Figure 15. Hydrate particle diameter varies with time under different activation energies.

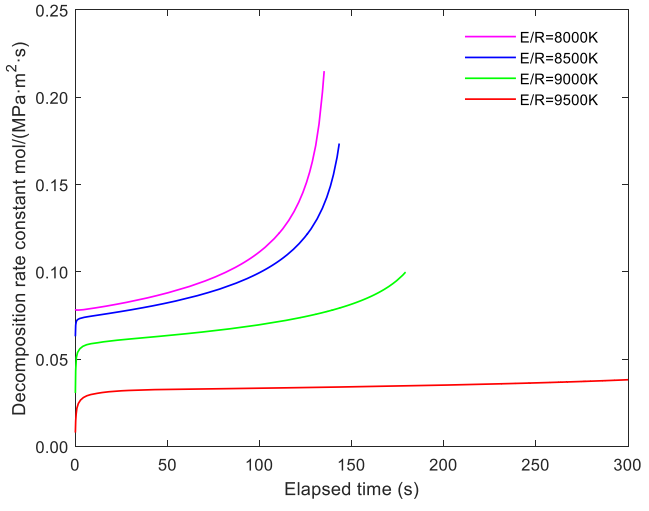

Figure 16. Hydrate particle decomposition rate constant varies with time under different activation energies.

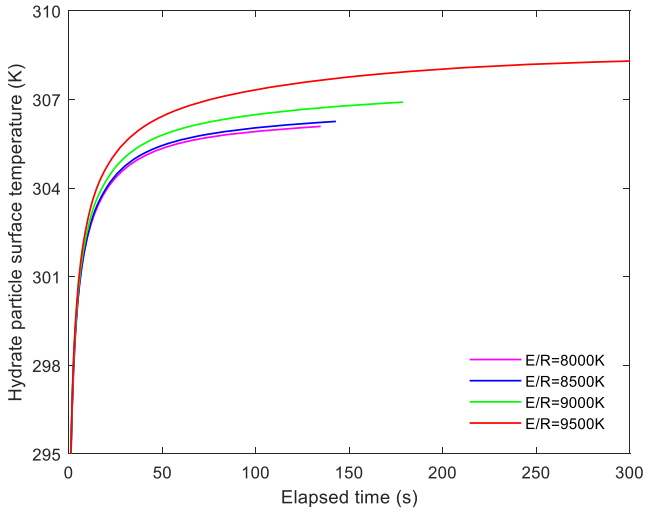

Figure 17. Hydrate particle surface temperature varies with time under different activation energies.

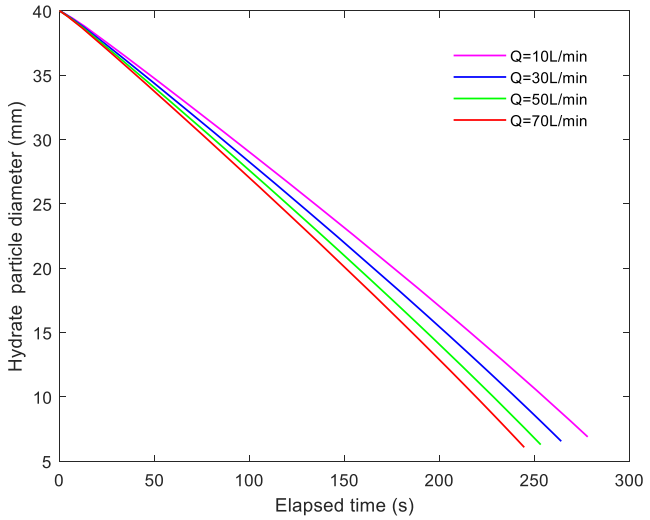

Figure 18. Hydrate particle diameter varies with time at different flowing rates.

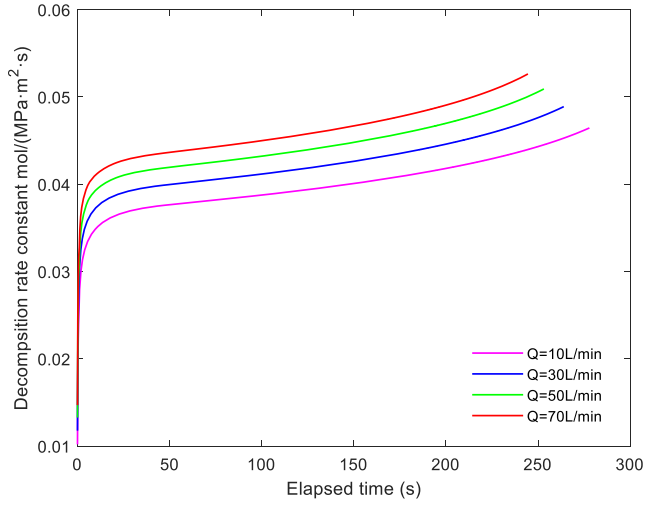

Figure 19. Hydrate particle decomposition rate constant varies with time at different flowing rates.

https://doi.org/10.1021/acsomega.1c03091
ACS Omega 2021, 6, 23355−23367

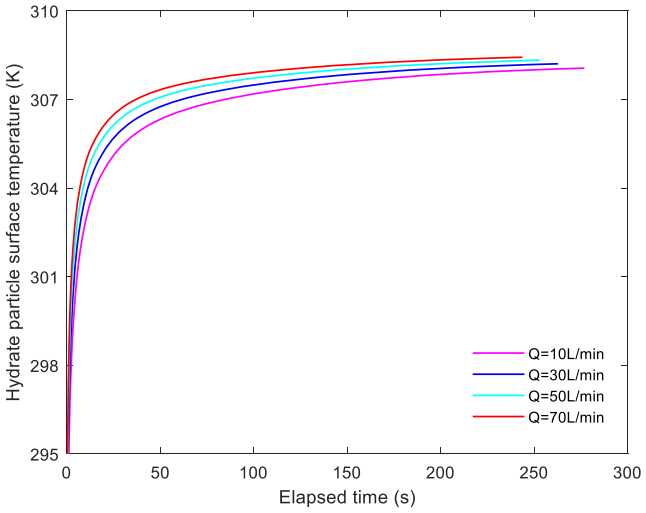

Figure 20. Hydrate particle surface temperature varies with time at different flowing rates.

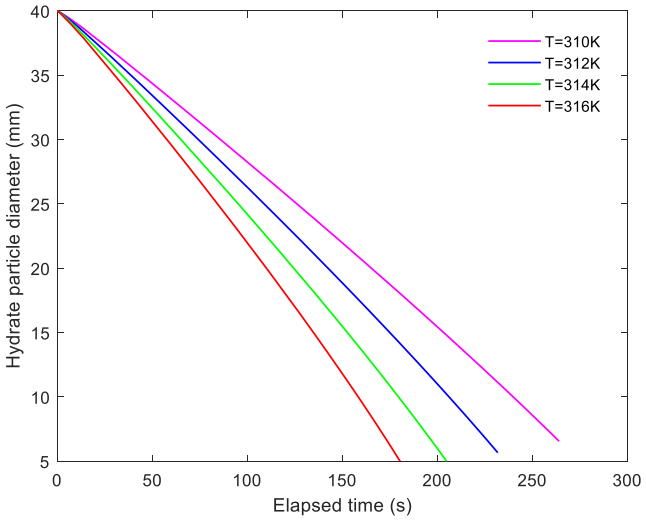

Figure 21. Hydrate particle diameter varies with time at different system temperatures.

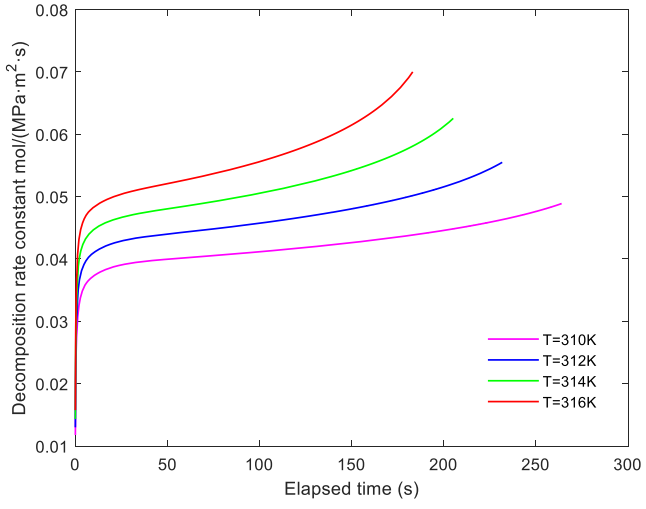

Figure 22. Hydrate particle decomposition rate constant varies with time at different system temperatures.

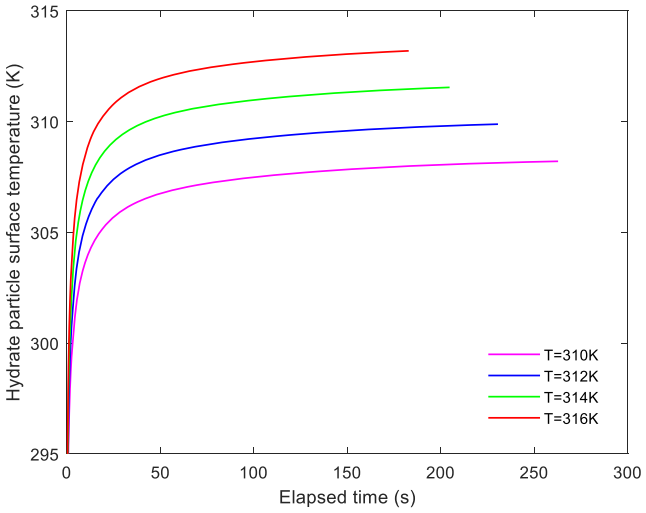

Figure 23. Hydrate particle surface temperature varies with time at different system temperatures.

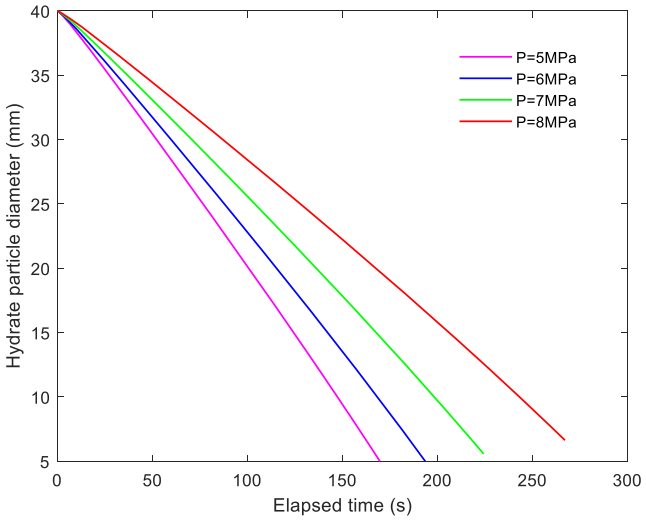

Figure 24. Hydrate particle diameter varies with time at different system pressures.

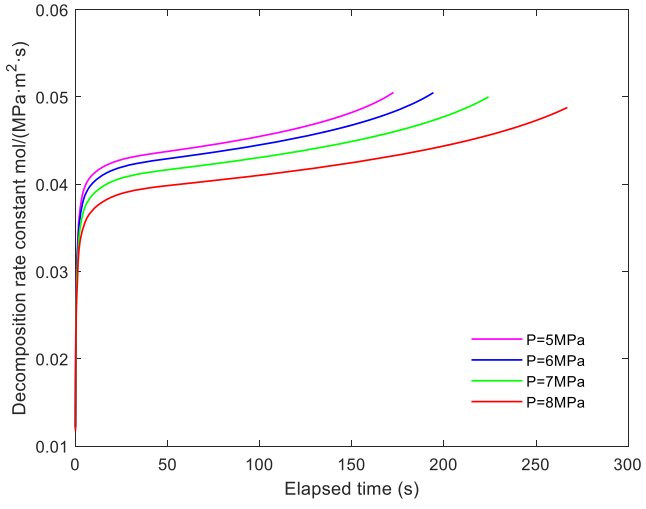

Figure 25. Hydrate particle decomposition rate constant varies with time at different system pressures.

https://doi.org/10.1021/acsomega.1c03091
ACS Omega 2021, 6, 23355−23367

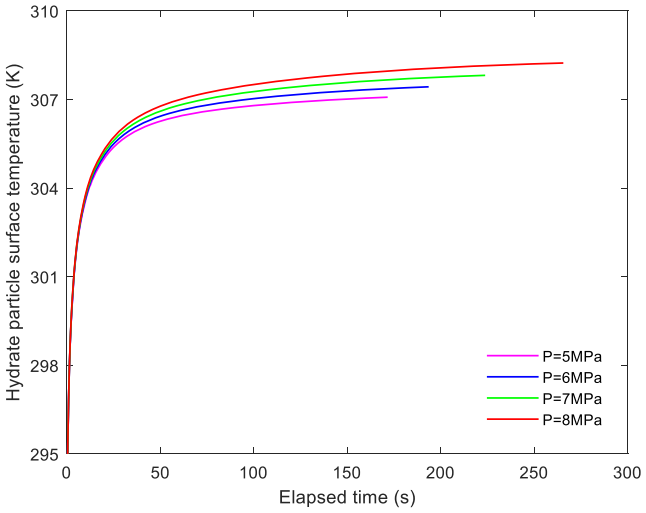

Figure 26. Hydrate particle surface temperature varies with time at different system pressures.

activation energy, water velocity, system temperature, and system pressure on the hydrate decomposition characteristics was analyzed. This paper draws the following conclusions through the study:

(1) The hydrate decomposition is a non-isothermal process, and the decomposition rate depends on the intrinsic kinetics, heat, and the mass transfer rate of the hydrate. At the initial stage of hydrate decomposition, the surface temperature of hydrate particles increases sharply, and the hydrate decomposition rate mainly depends on the heat transfer rate. In the late hydrate decomposition stage, the surface temperature of hydrate particles tends to be stable, and the hydrate decomposition rate depends on the hydrate intrinsic kinetics. By contrast, the mass transfer rate has little influence on the hydrate decomposition rate.

(2) The activation energy of the hydrate decomposition reaction has an important effect on the hydrate decomposition rate. The higher the activation energy, the faster the hydrate decomposition. When $E/R > 9000$ K, the hydrate decomposition rate constant decreases significantly. Besides, with the increase of water velocity, the intensity of heat convection increases, thus accelerating the decomposition of hydrate particles.

(3) System temperature and pressure are two major factors affecting the hydrate decomposition rate. With the increase of system temperature, the surface temperature of hydrate particles increases, and the heat transfer rate increases, thus speeding up hydrate decomposition. The decrease of system pressure directly increases the driving force of hydrate decomposition and increases the hydrate decomposition rate.

AUTHOR INFORMATION

Corresponding Author

Jun Li − *China University of Petroleum (Beijing), Beijing 102249, China; China University of Petroleum (Beijing) at Karamay, Karamay 834000, China*; Email: lijun446@vip.163.com

Authors

Geng Zhang − *China University of Petroleum (Beijing), Beijing 102249, China*; orcid.org/0000-0002-1601-0479

Gonghui Liu − *China University of Petroleum (Beijing), Beijing 102249, China*

Hongwei Yang − *China University of Petroleum (Beijing), Beijing 102249, China*

Honglin Huang − *China University of Petroleum (Beijing), Beijing 102249, China*

Complete contact information is available at: https://pubs.acs.org/10.1021/acsomega.1c03091

Notes

The authors declare no competing financial interest.

ACKNOWLEDGMENTS

The work was supported by the National Natural Science Foundation of China (no. 51734010) and the Science Foundation of China University of Petroleum, Beijing (no.2462020XKBH011).

NOMENCLATURE

n	molar amount of hydrate, mol
t	time, s
t_{in}	time for hydrate particles to begin to decompose, s
k_{hyd}	hydrate decomposition rate constant, mol/(MPa·m^2·s)
k_{hydc}	hydrate intrinsic decomposition rate, mol/(MPa·m^2·s)
k_{hydf}	mass transfer rate, mol/(MPa·m^2·s)
k^0_{hydc}	hydrate intrinsic decomposition rate constant, mol/(MPa·m^2·s)
k^0_{hydf}	mass transfer rate constant, mol/(MPa·m^2·s)
A	dissociation surface area of hydrate, m^2
f_{eq}	equilibrium fugacity, MPa
f	fugacity, MPa
T	temperature, K
T_{eq}	equilibrium temperature, MPa
T_w	water temperature, K
T_s	surface temperature of hydrate particle, K
T_{init}	initial temperature of hydrate particle, K
T_c	critical temperature, K
T_r	reduced temperature, K
p	pressure, MPa
p_{eq}	equilibrium pressure, MPa
p_c	critical pressure, MPa
p_r	reduced pressure, MPa
E_{act}	activation energy, J/mol
R	gas constant, J/(mol·K)
n_{sh}	Sherwood numbers
n_{sc}	Schmidt numbers
Re	Reynolds numbers
d_s	hydrate particle diameter, mm
D_{AB}	diffusion coefficient, m^2/s
ν	water flowing rate, m/s
ρ	density, kg/m^3
μ	viscosity, Pa·s
Z	compression coefficient
c	specific heat capacity, J/(kg·K)
λ	heat conductivity coefficient, W/(m·K)
r	hydrate particle radius, m
Pr	Prandtl numbers
Nu	Nusselt numbers
ΔH_h	heat of hydrate decomposition, J/kg
S	source term
M	molar mass of hydrate, kg/mol
θ	spherical coordinates, azimuth

https://doi.org/10.1021/acsomega.1c03091
ACS Omega 2021, 6, 23355−23367

φ spherical coordinate elevation
L distance from the center of the hydrate particle to the surface, m
i ith node
i_0 mesh adjustment factor
m total number of nodes

SUBSCRIPTS

g gas
l liquid
h hydrate

REFERENCES

(1) Yin, Z.; Linga, P. Methane hydrates: A future clean energy resource. *Chin. J. Chem. Eng.* **2019**, *27*, 2026−2036.
(2) Collett, T.; Bahk, J.-J.; Baker, R.; Boswell, R.; Divins, D.; Frye, M.; Goldberg, D.; Husebø, J.; Koh, C.; Malone, M.; et al. Methane Hydrates in Nature-Current Knowledge and Challenges. *J. Chem. Eng. Data* **2015**, *60*, 319−329.
(3) Song, Y.; Yang, L.; Zhao, J.; Liu, W.; Yang, M.; Li, Y.; Liu, Y.; Li, Q. The status of natural gas hydrate research in China: A review. *Renew. Sustain. Energy Rev.* **2014**, *31*, 778−791.
(4) Seol, J.; Lee, H. Natural gas hydrate as a potential energy resource: From occurrence to production. *Korean J. Chem. Eng.* **2013**, *30*, 771−786.
(5) Li, F.; Yuan, Q.; Li, T.; Li, Z.; Sun, C.; Chen, G. A review: Enhanced recovery of natural gas hydrate reservoirs. *Chin. J. Chem. Eng.* **2019**, *27*, 2062−2073.
(6) Feng, Y.; Chen, L.; Suzuki, A.; Kogawa, T.; Okajima, J.; Komiya, A.; Maruyama, S. Enhancement of gas production from methane hydrate reservoirs by the combination of hydraulic fracturing and depressurization method. *Energy Convers. Manag.* **2019**, *184*, 194−204.
(7) Zhang, J.; Sun, Q.; Wang, Z.; Wang, J.; Sun, X.; Liu, Z.; Sun, B..; Sun, J. Prediction of hydrate formation and plugging in the trial production pipes of offshore natural gas hydrates. *J. Clean. Prod.* **2021**, *316*, 128262.
(8) Jian, B.; Zhang; Zhi, Y.; Wang; Shun, L..; Wei, G.; Zhang; Jing, Yu.; Sun, B. Prediction of hydrate deposition in pipelines to improve gas transportation efficiency and safety. *Appl. Energy* **2019**, *253*, 113521.
(9) Zhang, J.; Wang, Z.; Duan, W.; Fu, W.; Sun, B.; Sun, J.; Tong, S. Real-Time Estimation and Management of Hydrate Plugging Risk During Deepwater Gas Well Testing. *SPE J.* **2020**, *25*, 3250−3264.
(10) Bayles, G. A.; Sawyer, W. K.; Anada, H. R.; Reddy, S.; Malone, R. D. A Steam Cycling Model for Gas Production from a Hydrate Reservoir. *Chem. Eng. Commun.* **1986**, *47*, 225−245.
(11) Holder, G. D.; Angert, P. F.; John, V. T.; Yen, S. A Thermodynamic Evaluation of Thermal Recovery of Gas From Hydrates in the Earth (includes associated papers 11863 and 11924). *J Pet Technol* **1982**, *34*, 1127−1132.
(12) Kamath, V. A.; Holder, G. D. Dissociation heat transfer characteristics of methane hydrate. *AIChE J.* **1987**, *33*, 347−350.
(13) Selim, M. S.; Sloan, E. D. Heat and mass transfer during the dissociation of hydrates in porous media. *AIChE J.* **1989**, *35*, 1049−1052.
(14) Kim, H. C.; Bishnoi, P. R.; Heidemann, R. A.; Rizvi, S. S. H. Kinetics of methane hydrate decomposition. *Chem. Eng. Sci.* **1987**, *42*, 1645−1653.
(15) Jamaluddin, A. K. M.; Kalogerakis, N.; Bishnoi, P. R. Modelling of decomposition of a synthetic core of methane gas hydrate by coupling intrinsic kinetics with heat transfer rates. *Can. J. Chem. Eng.* **1989**, *67*, 948−954.
(16) Hong, H.; Pooladi-Darvish, M.; Bishnoi, P. R. Analytical modeling of gas production from hydrates in porous media. *J. Can. Petrol. Technol.* **2003**, *42*, 45−56.
(17) Oyama, H.; Konno, Y.; Masuda, Y.; Narita, H. Dependence of depressurization induced dissociation of methane hydrate bearing laboratory cores on heat transfer. *Energy Fuel.* **2009**, *23*, 4995−5002.
(18) Sean, W.-Y.; Sato, T.; Yamasaki, A.; Kiyono, F. CFD and experimental study on methane hydrate dissociation Part I. Dissociation under water flow. *AIChE J.* **2007**, *53*, 262−274.
(19) Hamaguchi, R.; Nishimura, Y.; Inoue, G.; Matsukuma, Y.; Minemoto, M. Gas hydrate decomposition rate in flowing water. *J. Energy Resour. Technol.* **2007**, *129*, 102−106.
(20) Turner, D. J. *Clathrate hydrate formation in water-in-oil dispersions*; Academic Press: Golden State, US, 2005, pp 1−35.
(21) Joshi, S. V.; Grasso, G. A.; Lafond, P. G.; Rao, I.; Webb, E.; Zerpa, L. E.; Sloan, E. D.; Koh, C. A.; Sum, A. K. Experimental flowloop investigations of gas hydrate formation in high water cut systems. *Chem. Eng. Sci.* **2013**, *97*, 198−209.
(22) Zerpa, L. E.; Rao, I.; Aman, Z. M.; Danielson, T. J.; Koh, C. A.; Sloan, E. D.; Sum, A. K. Multiphase flow modeling of gas hydrates with a simple hydrodynamic slug flow model. *Chem. Eng. Sci.* **2013**, *99*, 298−304.
(23) Shi, B.; Ding, L.; Liu, Y.; Yang, J.; Song, S.; Wu, H.; Wang, W.; Gong, J. Hydrate slurry flow property in W/O emulsion systems. *RSC Adv.* **2018**, *8*, 11436−11445.
(24) Gao, Y.; Cui, Y.; Xu, B.; Sun, B.; Li, H.; Chen, L. Two phase flow heat transfer analysis at different flow patterns in the wellbore. *Appl. Therm. Eng.* **2017**, *117*, 544−552.
(25) Dzyuba, A. V.; Zektser, I. S. Variations in submarine groundwater runoff as a possible cause of decomposition of marine methane-hydrates in the Arctic. *Water Resour.* **2013**, *40*, 74−83.

https://doi.org/10.1021/acsomega.1c03091
ACS Omega 2021, 6, 23355−23367